Density Gradient Stabilization of Electron Temperature Gradient Driven Turbulence in a Spherical Tokamak

Y. Ren, S. M. Kaye, E. Mazzucato, W. Guttenfelder, R. E. Bell, C. W. Domier, B. P. LeBlanc, K. C. Lee, N. C. Luhmann, Jr., D. R. Smith, and H. Yuh

Density Gradient Stabilization of Electron Temperature Gradient Driven Turbulence in a Spherical Tokamak

Y. Ren,[1] S. M. Kaye,[1] E. Mazzucato,[1] W. Guttenfelder,[1] R. E. Bell,[1] C. W. Domier,[2]

B. P. LeBlanc,[1] K.C. Lee,[2] N. C. Luhmann, Jr.,[2] D. R. Smith,[3] and H. Yuh[4]

[1]*Princeton Plasma Physics Laboratory, Princeton, NJ 08543*
[2]*University of California at Davis, Davis, CA 95616*
[3]*University of Wisconsin-Madison, Madison, WI,53706*
[4]*Nova Photonics, Inc., Princeton, NJ 08540*

Abstract

In this letter we report the first clear experimental observation of density gradient stabilization of electron temperature gradient driven turbulence in a fusion plasma. It is observed that longer wavelength modes, $k_\perp \rho_s \lesssim 10$, are most stabilized by density gradient, and the stabilization is accompanied by about a factor of two decrease in the plasma effective thermal diffusivity.

PACS numbers: Valid PACS appear here

Micro-instabilities in fusion plasmas, *e.g.* Ion Temperature Gradient (ITG) mode, Trapped Electron Mode(TEM) and Electron Temperature Gradient (ETG) mode, could drive micro-turbulence, a major candidate in producing anomalous transport. Understanding, and thus controlling micro-instabilities is one of the most challenging problems in the controlled magnetic fusion research. In the literature, the density gradient has been predicted to be able to stabilize ITG, ETG, but to stabilize or destabilize TEM depending on collisionality [1]. The stability of these micro-instabilities can be quantified by the critical temperature gradient at which an instability is marginally unstable. For example, an analytic form of the critical temperature gradient for ETG instability is derived as in Ref. [2]:

$$(R_0/L_{T_e})_{crit} = max\{(1 + Z_{eff}\frac{T_e}{T_i})(1.33 + 1.99\hat{s}/q)(...), 0.8R_0/L_{n_e}\} \tag{1}$$

where R_0 is the major radius of the flux surface center, $L_{T_e} = (dlnT_e/dr)^{-1}$ is the electron temperature scale length, $L_{n_e} = (dlnn_e/dr)^{-1}$ is the electron density scale length, Z_{eff} is the effective ionic charge, T_e is the electron temperature, T_i is the ion temperature, $\hat{s} = (r/q)(dq/dr)$ is the magnetic shear, q is the magnetic safety factor, and (...) denotes some geometric terms not easily quantifiable for low aspect ratio tokamaks. It can be seen from this formula that if large enough, the density gradient term, $0.8R_0/L_{n_e}$, could determine the critical temperature gradient alone and result in the stabilization of ETG modes. Confinement improvements have been observed to be associated with peaked density profile resulting from pellet injection [3], and the improvements were attributed to density gradient, perpendicular flow shearing and/or reversed magnetic shear [4–6]. Here we present the first direct experimental demonstration of density gradient stabilization of electron-gyro scale turbulence. The experimental observation is in quantitative agreement with linear numerical simulations and supports the conclusion that the observed density fluctuations are driven by ETG. Furthermore, it is found that the longer wavelength modes, $k_\perp\rho_s \lesssim 10$ (ρ_s is the ion gyroradius at electron temperature and $k_\perp$ is the wavenumber perpendicular to local equilibrium magnetic field), are strongly stabilized by density gradient and that plasma effective thermal diffusivity is decreased by about a factor of two along with the stabilization.

The measurement was carried out on National Spherical Torus Experiment (NSTX) with a 280 GHz collective microwave scattering system (the high-k scattering system) [7]. This

2

scattering system has five channels covering a wavenumber range of 5 cm^{-1} $\lesssim k_\perp \lesssim 30$ cm^{-1} with a wavenumber resolution about 1 cm^{-1} and a radial resolution of $\triangle R \approx \pm 2$ cm, which allows us to study the evolution of local fluctuation with respect to local equilibrium quantities, $e.g.$ L_{T_e}, L_{n_e}, q and $\hat{s}$.
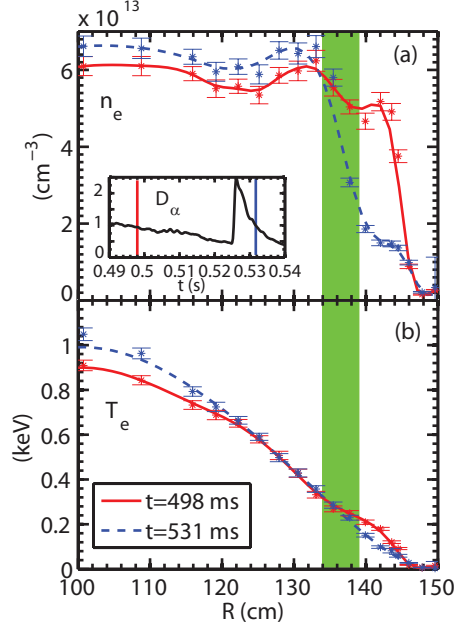

FIG. 1: (a) Radial profiles of electron density at $t = 498$ and 532 ms which are before and after an ELM event (see the inserted D_α signal, where the two vertical lines denote the two Thompson time points); (b) Radial profiles of electron temperature at $t = 498$ and 532 ms. The shaded regions denote the measuring region of the high-k system. Large change in L_{n_e} after the ELM at $t = 532$ ms is evident.

Figure 1 shows the density (a) and temperature (b) profiles at t=498 ms (before an ELM event [8]) and at t=532 ms (after the ELM event) measured by Multiple Point Thompson Scattering (MPTS) [9] of shot 140620, a deuterium H-mode plasma with 900 kA plasma current and 4.5 kG toroidal field. The measurement region of the high-k scattering system, the overall radial region covered by all channels with the center of scattering location separated by $\lesssim 1$ cm, is from about $R = 134$ to 139 cm. A large increase in density gradient after the ELM event in the measurement region is evident in Fig. 1(a) and only small change in electron temperature profile is seen in Fig. 1(b). We also note that magnetic measurements show no large amplitude global MHD activity before, during and right after the ELM event.

Figure 2 shows the spectrograms of channels 2 and 3 of the high-k system and the
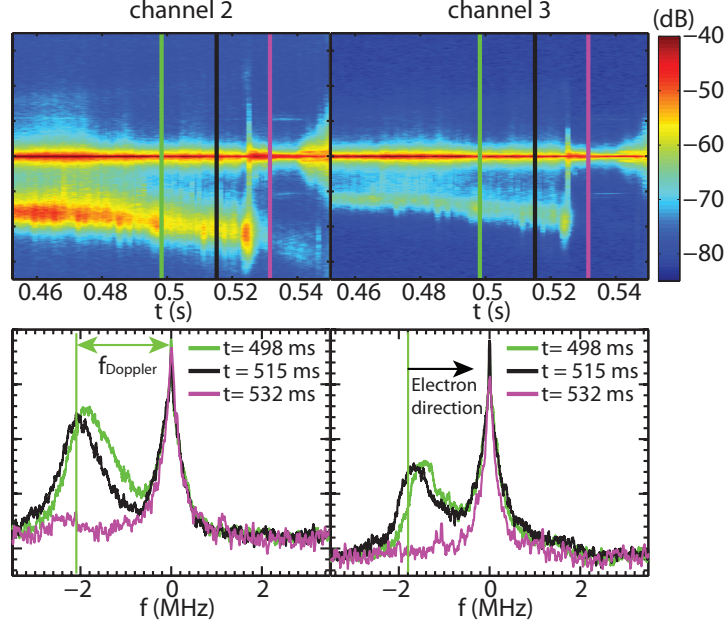
FIG. 2: Upper panels: The spectrograms of two high-k channels around the ELM event; Lower panels: The frequency spectra at the three exact MPTS time points, $t = 498$, 515 and 532 ms, for the two high-k channels. The three colored lines in the upper panels denote time points used for plotting the lower panels with the same color coding.

frequency spectra at three MPTS time points, $t = 498$, 515 (before the ELM event) and 532 ms (after the ELM event). The wavenumbers measured by the two channels are $k_\perp \rho_s \approx 10 - 12$ (channel 2) and $8 - 10$ (channel 3) before the ELM event, and become $15 - 17$ and $12.5 - 14.5$ after the ELM event due to a larger refraction following the ELM event. The signal from the collective scattering of microwave by electron density fluctuations manifests as spectral peaks at negative frequencies, corresponding to the ion diamagnetic direction in the laboratory frame. However, accounting for a Doppler shift of $k_T V_T / 2\pi$ (the vertical green lines in the lower panels denote $k_T V_T / 2\pi$ at $t = 498$ ms), where k_T is the toroidal wavenumber and V_T is the plasma toroidal flow, the wave propagation direction in the plasma frame is in the electron diamagnetic direction, consistent with previous results [10]. The large central peaks at $f = 0$ are due to the spurious reflection of the probing microwave beam, and large frequency separations between the scattering signals and the central peaks ensure accurate measurements of scattered microwave power. It can be immediately seen from the figure that the two channels show large reduction in scattering signal power after the ELM event, and most notably, the scattering signals received by channel 3 is below its

4

noise level. However, since the wavenumbers measured by the high-k channels increase after the ELM event, the change of wavenumber spectrum has to be assessed as below.
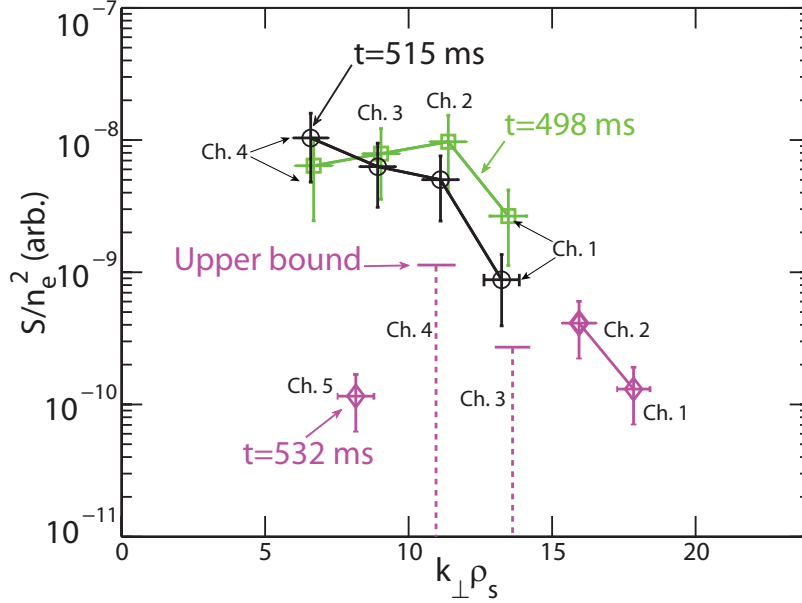

FIG. 3: The $k_\perp$ spectra in arbitrary unit (normalized to n_e^2 and S is the spectral density calculated using the total scattered power in the spectra of each channel) at the three MPTS time points. Data points are also labeled with their corresponding channel numbers. The absolute upper bounds for the density fluctuation spectral power are denoted by horizontal solid lines on the tops of vertical dashed lines.

Figure 3 shows the normalized $k_\perp$ spectra in arbitrary unit at the three MPTS time points. At $t = 532$ ms, estimated upper bounds are plotted for channels 3 and 4, since they have scattering signals below the noise level. The upper bounds of possible fluctuation power are estimated by using the scattering signal power of channel 5 at $t = 532$ ms, which is about three times higher than noise level, to obtain a minimum detectable scattering power (channel 5 has similar noise level as channels 3 and 4). It is clear from Fig. 3 that after the ELM event, *i.e.* at $t = 532$ ms, the fluctuation power for $k_\perp \rho_s \lesssim 15$ is reduced and the most significant reduction, more than an order of magnitude, occurs at small wavenumbers, $k_\perp \rho_s \lesssim 10$. We note that the actual reduction in spectral power in channels 3 and 4 could be more than denoted by the upper bounds. Interestingly, the fluctuation power at higher wavenumbers, $k_\perp \rho_s \gtrsim 15$, seems to be unaffected by the increase of density gradient, *i.e.* overlap in fluctuation power is expected if one extrapolates the $k_\perp$ spectrum at $t = 515$ ms

5

with a power law to higher wavenumbers. We also note that channel 5 is not included in the two $k_\perp$ spectra before the ELM event since for those particular density profiles, its scattering location is separated for more than 2 cm from those of the other four channels. However, this channel is included in the $k_\perp$ spectrum at $t = 532$ ms since the change of density profile after the ELM event leads to a better overlap of the radial scattering locations of different channels with separations of the center of scattering location $\lesssim 1$ cm.
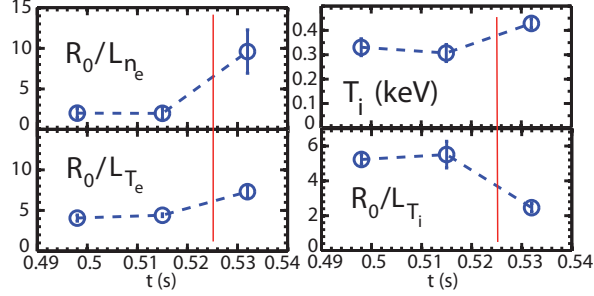

FIG. 4: The normalized electron density gradient, R_0/L_{n_e}, normalized electron temperature gradient, R_0/L_{T_e}, ion temperature, T_i and normalized ion temperature gradient, R_0/L_{T_i}, at $t = 498$, 515 and 532 ms averaged in the high-k measurement locations (see main text). The timing of the ELM event is denoted by the red vertical solid lines.

In order to demonstrate the fact that the density gradient has the largest change (increase) in the high-k measurement region after the ELM event, the time evolutions of four equilibrium quantities around the ELM event are plotted at the three MPTS time points in Fig. 4. The error bars in the figure represent profile variations in high-k measurement regions for channels measuring the wavenumbers experiencing the largest change in spectral power after the ELM event, namely Channels 3 and 4 before the ELM event (from about $R = 134.5$ to 138.5 cm) and channels 4 and 5 after the ELM event (from about $R = 134$ to 138 cm). The normalized electron density gradient, R_0/L_{n_e}, and normalized electron temperature gradient, R_0/L_{T_e}, are obtained from the MPTS profiles. T_i and normalized ion temperature gradient, R_0/L_{T_i} are obtained from charge exchange recombination spectroscopy (CHERS) measurement [11]. It is easy to see from Fig. 4 that the greatest change in the equilibrium quantities after the ELM event is the factor of five increase of R_0/L_{n_e}. The next largest changes are the 60 percent increase in R_0/L_{T_e} and the 60 percent decrease in R_0/L_{T_i}. Despite the increase in the T_e gradient which drives ETG modes, the turbulence spectral power has been shown to be significantly decreased as shown in Fig. 3. The de-

6

crease in R_0/L_{T_i} should only affect the stability of ITG modes. However, the observation of neoclassical ion transport level in NSTX H-mode plasmas indicates that ITG modes are stabilized by geometrical and $E \times B$ shear effects [12]. In addition to changes in gradients, a 40 percent increase in T_i decreases T_e/T_i (T_e change is smaller), a destabilizing effect as shown in Eqn. 1. However, we will show later that the density gradient change is so large that as described in Eqn. 1, the second term in the "max" function overcomes the first term. Finally, we note that all other relevant equilibrium quantities, T_e, n_e, $\hat{s}$, q, Z_{eff} and the Hahm-Burrell $E \times B$ shear rate [13] show less than 25 percent change after the ELM event.
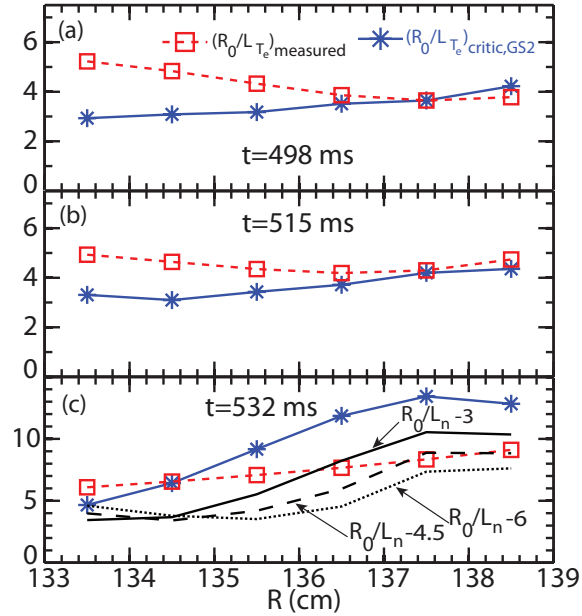

FIG. 5: The critical T_e gradients calculated by GS2, $(R_0/L_{T_e})_{critic,GS2}$, (asterisks) in comparison with the measured temperature gradient, $(R_0/L_{T_e})_{measured}$, (open squares) in the high-k measurement region: (a) at $t = 498$ ms; (b) $t = 515$ ms; (c) $t = 532$ ms. Additional lines in (c) denote $(R_0/L_{T_e})_{critic,GS2}$ calculated with $(R_0/L_{n_e} - 3)$ (solid line), $(R_0/L_{n_e} - 4.5)$ (dashed line) and $(R_0/L_{n_e} - 6)$ (dotted line).

The observed density gradient stabilization is in good agreement with stability analysis performed with the GS2 code [14]. GS2 is an initial value gyrokinetic code which, in its linear mode, finds the fastest growing mode for a given pair of poloidal and radial wavenumbers. In order to find the critical temperature gradient, growth rates of a range of unstable poloidal wavenumbers are calculated with several different temperature gradients.

7

Linear extrapolation of the growth rate of the most unstable mode determines the critical temperature gradient [2]. In Fig. 5, the critical T_e gradients in the high-k measurement region were calculated using GS2 and are plotted for the three MPTS time points, *i.e.* Fig. 5(a), (b), (c), together with measured T_e gradient profile. It can be seen from Fig. 5 that at the time points before the ELM event, *i.e.* 498 ms (a) and 515 ms (b), the measured T_e gradients are larger than the critical T_e gradients from GS2 calculation in most of the high-k measurement region. However, at $t = 532$ ms (c), after the ELM event, the critical T_e gradient from GS2 calculations is much larger than the measured T_e gradient for most of the high-k measurement region, *i.e.* ETG modes are linearly stable, which is able to explain the observed large reduction of spectral power for $k_\perp \rho_s < 10$ at $t = 532$ ms as shown in Fig. 3. We note that due to the small size of the existing ETG unstable region, where $(R_0/L_{T_e})_{measured} > (R_0/L_{T_e})_{critic,GS2}$, in Fig. 5 (c), it may not be enough to explain the unaffected spectral power for $k_\perp \rho_s \gtrsim 15$ in Fig. 3. In order to show that the density gradient increase is responsible for the large increase of critical T_e gradient in Fig. 5(c), critical T_e gradients calculated with R_0/L_{n_e} decreased by 3, 4.5 and 6 units are also plotted in Fig. 5 (c). It is clear that $(R_0/L_{n_e} - 3)$ leads to significantly lowered critical T_e gradients in the high-k measurement region. However, while the decreases to $(R_0/L_{n_e} - 4.5)$ and $(R_0/L_{n_e} - 6)$ lead to further reduction of critical R_0/L_{T_e} at $R > 135.5$ cm, only small change in critical R_0/L_{T_e} is observed at $R \lesssim 135$ cm, which is consistent with that the first term in the "max" function of Eqn. 1 dominates the critical R_0/L_{T_e} as the second density gradient term becomes sufficiently small.

The stabilization of the electron-scale turbulence is also found to be accompanied by an improvement in plasma confinement. The transport analysis was carried out with TRANSP [15]. Because of a strong energy coupling between electrons and ions due to large plasma density ($n_e \sim 5 \times 10^{19} m^{-3}$), here we show the plasma effective thermal diffusivity, χ, in Fig. 6 as a function of R at the three MPTS time points: $t = 498$, 515 and 532 ms, where a factor of about two reduction in χ can be seen in the high-k measurement regions used in Fig. 4 at $t = 532$ ms after the ELM event. (We note that the uncertainty in χ in the shaded region in Fig. 6 is about 30 percent). This correlation suggests that the reduction in the longer wavelength modes, $k_\perp \rho_s < 10$, may be responsible for the improvement in plasma confinement.

In conclusion, we have demonstrated the density gradient stabilization of electron-scale
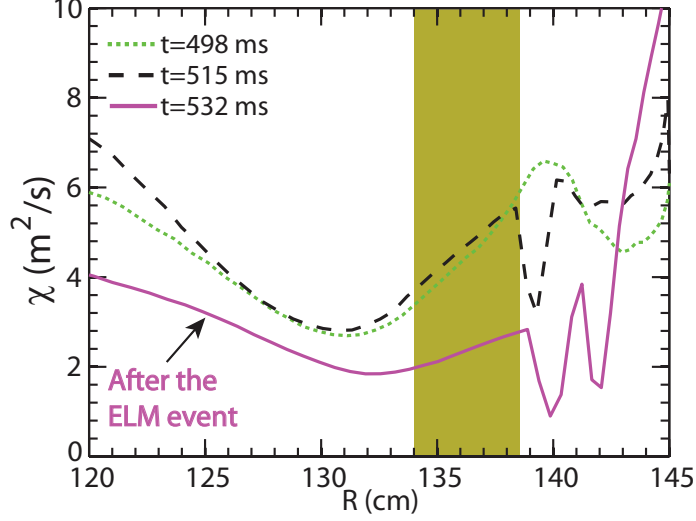
FIG. 6: The plasma effective thermal diffusivity as a function of R for the three MPTS time points: $t = 498$ (dotted line), 515 (dashed line) and 532 ms (solid line) with the shaded region denoting the high-k measurement regions as used in Fig. 4 (from about $R = 134$ to 138.5 cm).

turbulence by showing significant reduction in density fluctuation spectral power at $k_\perp \rho_s \lesssim$ 10 following a large density gradient increase induced by an ELM event. This observation together with linear gyrokinetic stability analysis supports that the turbulence we observe before the ELM event is driven by ETG instability. TEM, on the other hand, is ruled out by this observation, since our ion-scale GS2 calculations (not shown) shows that TEM should be destabilized by the large density gradient. A reduction in plasma effective thermal diffusivity is also found to be correlated with the significant reduction of spectral power at $k_\perp \rho_s \lesssim 10$, suggesting the importance of these modes in driving anomalous plasma thermal diffusion.

[1] F. Romanelli and S. Briguglio, Phys. Fluids B **2**, 754 (1990).

[2] F. Jenko *et al.*, Phys. Plasmas **8**, 4096 (2001).

[3] M. Greenwald *et al.*, Phys. Rev. Lett. **53**, 352 (1984).

[4] B. Balet *et al.*, Nucl. Fusion **30**, 2029 (1990).

[5] P. Maget *et al.*, Nucl. Fusion **39**, 949 (1999).

[6] M. Romanelli *et al.*, Phys. Plasmas **11**, 3845 (2004).

[7] D. R. Smith *et al.*, Rev. Sci. Instrum. **79**, 123501 (2008).

[8] H. Zohm, Plasma Phys. Control. Fusion **38**, 105 (1996).

[9] B. P. LeBlanc *et al.*, Rev. Sci. Instrum. **74**, 1659 (2003).

[10] E. Mazzucato *et al.*, Phys. Rev. Lett. **101**, 075001 (2008).

[11] R. E. Bell, Rev. Sci. Instrum. **77**, 10E902 (2006).

[12] S. M. Kaye *et al.*, Phys. Rev. Lett. **98**, 175002 (2007).

[13] T. S. Hahm and K. H. Burrell, Phys. Plasmas **2**, 1648 (1995).

[14] M. Kotschenreuther *et al.*, Comp. Phys. Comm. **88**, 128 (1995).

[15] R. J. Hawryluk, *Physics of Plasma Close to Thermonuclear Conditions* (Pergamon, New York, 1981).